DYNAMICS OF FLEXIBLE MANIPULATORS

A. Meghdari and M. Ghassempouri
Department of Mechanical Engineering
Sharif University of Technology
Tehran, Iran

Abstract This paper presents an application of Continuum (i.e. Lagrangian) and Finite Element Techniques to flexible manipulator arms for derivation of the corresponding Dynamic Equations of Motion. Specifically a one-link flexible arm is considered for detailed analysis, and the results are extended for the case of a two-link flexible manipulator. Numerical examples are given for the case of both one and two link flexible arms, and the resulting dynamic equations are solved and thoroughly discussed. In addition, both methods are compared in the sense of modeling and the required time and accuracy for computation.

Key Words Continuum Dynamic Equation, Finite Element, Flexible Manipulators.

چکیده این مقاله کاربردی از روشهای پیوسته (لاگرانژین) واجزاء محدود را در بدست آوردن معادلات دینامیکی بازوهای مکانیکی الاستیک ارائه می دهد. ابتدا یک بازوی مکانیکی الاستیک یک اتصاله برای تحلیلی جامع درنظر گرفته شده است. سپس نتایج حاصله به یک بازوی مکانیکی الاستیک دواتصاله بسط داده شده اند. در ادامه مثالهایی عددی برای هردو مورد از بازوهای مکانیکی یک و دو اتصاله درنظر گرفته شده و معادلات دینامیکی منتجّه حلّ و بحث گردیده اند. نهایتاً، هردو روش از نقطه نظر مدلسازی، مدّت زمان و دقّت محاسباتی نیز مورد مقایسه و تحلیل قرار گرفته اند.

INTRODUCTION

Recent advances in the design and control of robot manipulators clearly indicate the importance of robot structural flexibility and the fact that this study is still in its infancy. In the past several years researchers in this field have shown increasing interest in the modeling and analysis of link and joint flexibilities in computer controlled manipulators and robots. Currently, in order to circumvent the problem of robotic deformations the practice is to design a manipulator which is very rigid. This results in the creation of a heavy arm, that by itself puts more of a strain on the actuators that drive the manipulators joints and furthermore reduces the mobility of the robotic structure due to the large values of inertial forces. In addition, light weight manipulators are needed to increase robot operating speeds without requiring high performance actuators. The drawback of robots having lightweight arms is represented by their structural elasticity which makes modeling and control complicated tasks. Book et al. [1-4], Usoro et al. [5], Ghassempouri [6], and Meghdari [7] have made significant contributions to the modeling, design, and control of manipulators with elastic members. In the following sections, exact and approximate dynamic models of flexible manipulators are derived using the continuum and finite element methods and a comparative analysis of both models is presented.

PART ONE: ANALYTICAL MODELING

The Continuum Approach

In this section we make use of the Lagrangian technique presented by Book [1]. The presented model considers a robot manipulator consisting of elastic links, and rotary rigid joints. By defining two transformation matrices, one for expressing the joints' rotation and the other for expressing the links' elastic deformation, one can specify the position of any point on the manipulator at any configuration. Assuming small deflection in links, elastic deformation of each link would be equal to the sum of the assumed mode shapes.

Using the above assumptions, a suitable formulation for expressing the potential and kinetic energies of the system is found. Then, using the Hamiltonian principle

one can derive the equations of motion of the flexible manipulator.

In this paper, using the Lagrangian method, the nonlinear equations of motion for a one link planar robot are derived. This robot is capable of bending only in the plane of motion. Axial deformation and twisting of the robot's link are ignored in our analysis.

Kinematics of the Mechanism

The position of a point on the robot's link in Cartesian coordinates is defined by an augmented vector as:

[1, X-component, Y-component, Z-component]

Furthermore, the coordinate frame (X_1, Y_1, Z_1) is attached to the link with origin "O" at the joint, and it is oriented such that its X-axis is coincident with the neutral axis of the link in its undeformed condition (see Figure 1). When the link is undeformed a point on the neutral axis at $X = \eta$ is located at ${}^1\underset{\sim}{h}_1(\eta)$ under a general condition of deformation in terms of coordinate frame (X_1, Y_1, Z_1) as:

$$ {}^1\underset{\sim}{h}_1(\eta) = \begin{bmatrix} 1 \\ \eta \\ 0 \\ 0 \end{bmatrix} + \sum_{j=1}^{m} \delta_j(t) \begin{bmatrix} 0 \\ x_j(\eta) \\ y_j(\eta) \\ z_j(\eta) \end{bmatrix} \qquad (1) $$

where:

X_j, Y_j, Z_j = displacement components of mode j of the link

$\delta_j(t)$ = the time varying amplitude of mode j of the link; and

m = the number of modes used to describe the link deflection.

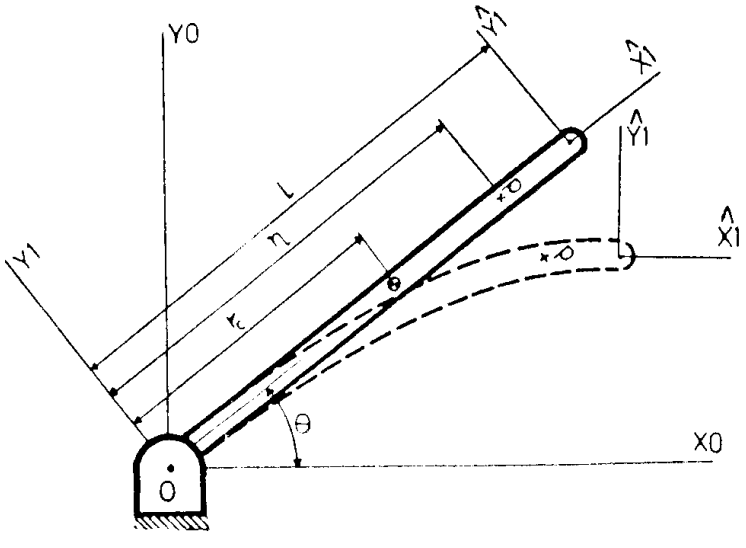

Figure 1. Schematics of a one-link flexible arm.

Let us further define the coordinate frame $(\hat{X}_1, \hat{Y}_1, \hat{Z}_1)$ fixed to the link such that in the case of no deformation it is parallel to the (X_1, Y_1, Z_1) coordinate system with X_1 and $\hat{X}_1$ being coincident. Hence, using a homogeneous transformation one can describe the position of a point in terms of the fixed base coordinate frame (X_0, Y_0, Z_0) as:

$$ \underset{\sim}{h}_1 = \underset{\approx}{w}_1 {}^1\underset{\sim}{h}_1 \qquad (2) $$

where:

$$ \underset{\approx}{w}_1 = \begin{bmatrix} 1 & 0 & 0 & 0 \\ 0 & C\theta & -S\theta & 0 \\ 0 & S\theta & C\theta & 0 \\ 0 & 0 & 0 & 1 \end{bmatrix} \qquad (3) $$

and $C\theta = \cos(\theta)$, $S\theta = \sin(\theta)$.

Therefore, the position of a point on the link in the base frame is given by:

$$ \underset{\sim}{h}_1 = \underset{\approx}{w}_1 {}^1\underset{\sim}{h}_1 = \begin{bmatrix} 1 \\ C\theta\left[\eta + \sum_{j=1}^{m} \delta_j(t) x_j(\eta)\right] - S\theta\left[\sum_{j=1}^{m} \delta_j(t) y_j(\eta)\right] \\ S\theta\left[\eta + \sum_{j=1}^{m} \delta_j(t) x_j(\eta)\right] + C\theta\left[\sum_{j=1}^{m} \delta_j(t) y_j(\eta)\right] \\ \left[\sum_{j=1}^{m} \delta_j(t) z_j(\eta)\right] \end{bmatrix} \qquad (4) $$

Please note that it is assumed the bending occurs in the XY plane, and the axial deformation is neglected; $X_j(\eta) = Z_j(\eta) = 0$. Thus we have:

$$ \underset{\sim}{h}_1 = \begin{bmatrix} \eta C\theta - S\theta\left[\sum_{j=1}^{m} \delta_j(t) y_j(\eta)\right] \\ \eta S\theta + C\theta\left[\sum_{j=1}^{m} \delta_j(t) y_j(\eta)\right] \end{bmatrix} $$

Furthermore, the link transformation matrix between (X_1, Y_1, Z_1) and $(\hat{X}_1, \hat{Y}_1, \hat{Z}_1)$ farmes can be expressed as:

$$\underset{\approx}{E} = \left[\underset{\approx}{H} + \sum_{j=1}^{m} \delta_j(t) \underset{\approx}{M_j} \right] \tag{5}$$

where:

$$\underset{\approx}{H} = \begin{bmatrix} 1 & 0 & 0 & 0 \\ l & 1 & 0 & 0 \\ 0 & 0 & 1 & 0 \\ 0 & 0 & 0 & 1 \end{bmatrix} \qquad \underset{\approx}{M_j} = \begin{bmatrix} 0 & 0 & 0 & 0 \\ \bar{x}_j & 0 & -\bar{\theta}_{zj} & \bar{\theta}_{yj} \\ \bar{y}_j & \bar{\theta}_{zj} & 0 & -\bar{\theta}_{xj} \\ \bar{z}_j & -\bar{\theta}_{yj} & \bar{\theta}_{xj} & 0 \end{bmatrix}$$

l = the link length,

$\bar{X}_j, \bar{Y}_j, \bar{Z}_j$ = displacement components of mode j of the link at $\eta = l$,

$\bar{\theta}_{xj}, \bar{\theta}_{yj}, \bar{\theta}_{zj}$ = rotational components of model j of the link at $\eta = l$.

Once again note that bending is assumed to occur in the XY plane as shown in Figure 1, and axial deformation is neglected; hence $\bar{\theta}_{xj} = \bar{\theta}_{yj} = 0$, and $\bar{X}_j = \bar{Z}_j = 0$.

The System's Kinetic Energy

The kinetic energy of a point on the link is given as:

$$dT = \frac{1}{2} dm \, Tr\left\{ \underset{\sim}{\dot{h}_1} . \underset{\sim}{\dot{h}_1}^T \right\} \tag{6}$$

where dm represents a differential mass at that point, and Tr{ } is the trace operator. For slender links we have:

$$dm = \mu \, d\eta$$

where μ is the mass per unit length.

Integrating Equation 6 over the link length results in the total kinetic energy contribution as:

$$T = \frac{1}{2} \int_0^l Tr\left\{ \underset{\sim}{\dot{h}_1} . \underset{\sim}{\dot{h}_1}^T \right\} \mu \, d\eta \tag{7}$$

which may be expressed as [1]:

$$T = Tr\left\{ \underset{\approx}{\dot{w}_1} \underset{\approx}{B_3} \underset{\approx}{\dot{w}_1}^T + 2 \underset{\approx}{\dot{w}_1} \underset{\approx}{B_2} \underset{\approx}{w_1}^T + \underset{\approx}{w_1} \underset{\approx}{B_1} \underset{\approx}{w_1}^T \right\} \tag{8}$$

where:

$$\underset{\approx}{B_1} = \frac{\mu}{2} \begin{bmatrix} 0 & 0 & 0 & 0 \\ 0 & 0 & 0 & 0 \\ 0 & 0 \left[\sum_{j=1}^{m} \sum_{k=1}^{m} \dot{\delta}_j(t) \dot{\delta}_k(t) \int_0^l y_j(\eta) \, y_k(\eta) \, d\eta \right] & 0 \\ 0 & 0 & 0 & 0 \end{bmatrix} \tag{9}$$

$$\underset{\approx}{B_2} = \frac{\mu}{2} \begin{bmatrix} 0 & 0 & \left[\sum_{j=1}^{m} \dot{\delta}_j(t) \int_0^l y_j(\eta) \, d\eta \right] & 0 \\ 0 & 0 & \left[\sum_{j=1}^{m} \dot{\delta}_j(t) \int_0^l \eta y_j(\eta) \, d\eta \right] & 0 \\ 0 & 0 \left[\sum_{j=1}^{m} \sum_{k=1}^{m} \delta_k(t) \dot{\delta}_j(t) \int_0^l y_j(\eta) \, y_k(\eta) \, d\eta \right] & 0 \\ 0 & 0 & 0 & 0 \end{bmatrix} \tag{10}$$

$$\underset{\approx}{B_3} = \frac{\mu}{2} \begin{bmatrix} \int_0^l d\eta & \int_0^l \eta d\eta \\ \int_0^l \eta d\eta & \int_0^l \eta^2 d\eta \\ \left[\sum_{j=1}^{m} \delta_j \int_0^l y_j(\eta) \, d\eta \right] & \left[\sum_{j=1}^{m} \delta_j \int_0^l \eta y_j(\eta) \, d\eta \right] \\ 0 & 0 \end{bmatrix}$$

$$\begin{bmatrix} \left[\sum_{j=1}^{m} \delta_j \int_0^l y_j(\eta) \, d\eta \right] & 0 \\ \left[\sum_{j=1}^{m} \delta_j \int_0^l \eta y_j(\eta) \, d\eta \right] & 0 \\ \left[\sum_{j=1}^{m} \sum_{k=1}^{m} \delta_j \delta_k \int_0^l y_j(\eta) \, y_k(\eta) \, d\eta \right] & 0 \\ 0 & 0 \end{bmatrix} \tag{11}$$

and,

$$\dot{\underset{\approx}{w}}_1 = \begin{bmatrix} 0 & 0 & 0 & 0 \\ 0 & -\dot{\theta}S\theta & -\dot{\theta}C\theta & 0 \\ 0 & \dot{\theta}C\theta & -\dot{\theta}S\theta & 0 \\ 0 & 0 & 0 & 0 \end{bmatrix} \qquad (12)$$

From Equations 8 through 12 one can obtain:

$$T = \frac{\mu}{2}\left\{\sum_{i=1}^{m}\sum_{j=1}^{m}\left[\dot{\delta}_i\dot{\delta}_j + \dot{\theta}^2\delta_i\delta_j\right]\int_0^l y_j(\eta)\, y_i(\eta)\, d\eta + 2\dot{\theta}\sum_{i=1}^{m}\dot{\delta}_i \right.$$

$$\left.\int_0^l \eta y_i(\eta) d\eta + \dot{\theta}^2\int_0^l \eta^2 d\eta\right\} \qquad (13)$$

The System's Potential Energy

The potential energy of this system is contributed to two effects. One being the system's elasticity, and the other is due to the gravitational field.

a) Potential Energy due to the System's Elasticity.

Since the considered model bends only in the plane of motion, the corresponding elastic potential energy of the lenght $d\eta$ is:

$$dv_e = \frac{1}{2} d\eta \left\{ EI_z \left(\frac{\partial\theta_z(\eta)}{\partial\eta}\right)^2\right\} \qquad (14)$$

where:

θ_z : rotation of neutral axis of the link at the point η in the Z-direction.

E : Young's Modulus of Elasticity of the link.

I_z : the link's cross-sectional area moment of inertia about the Z-axis.

Considering a truncated modal approximation of the link deformation, θ_z can be represented by a summation over the modal coefficients times the deflection variables as:

$$\theta_z(\eta) = \sum_{k=1}^{m} \delta_k(t)\theta_{zk}(\eta) \qquad (15)$$

Where $\theta_{zk}(\eta)$ is the angle about the Z-axis corresponding to the k-th mode of the link.

On the other hand, from mechanics of materials we have:

$$\theta_{zk}(\eta) = \frac{\partial y_k(\eta)}{\partial\eta} \qquad (16)$$

and from Equations 14, 15, and 16 one can obtain:

$$dV_e = \frac{1}{2} d\eta \left\{ EI_z \left[\sum_{k=1}^{m} \delta_k(t)\left(\frac{\partial^2 y_k(\eta)}{\partial\eta^2}\right)\right]^2\right\} \qquad (17)$$

Finally integrating Equation 17 over the link length provides us with the Link's Total Elastic Potential Energy as:

$$V_e = \frac{1}{2}\left[\sum_{k=1}^{m}\sum_{l=1}^{m}\delta_k(t)\delta_l(t)EI_z\int_0^l \frac{\partial^2 y_k(\eta)}{\partial\eta^2}\cdot\frac{\partial^2 y_l(\eta)}{\partial\eta^2} d\eta\right] \qquad (18)$$

b) Potential Energy Due to Gravity

Considering a differential element of length $d\eta$ on the link, the potential energy due to gravity can be written as:

$$dV_g = -\mu \underset{\sim}{g}^T \underset{\approx}{w}_1^1 \underset{\sim}{h}_1 d\eta \qquad (19)$$

where the gravity vector g has the form:

$$\underset{\sim}{g}^T = [0, g_x, g_y, g_z]$$

Note that in our model $g_x = g_z = 0$, and $g_y = -g$. Integrating Equation 19 over the link length, the resulting Gravitational Potential Energy is:

$$V_g = -Mg_y r_c S\theta - g_y \mu C\theta \sum_{k=1}^{m} \delta_k(t)\int_0^l y_k(\eta)\, d\eta \qquad (20)$$

Where:

M : is the total mass of the link, and

r_c : is the distance from the undeformed center of gravity to point 0.

Lagrangian Equations of Motion

Utilizing the general form of the Lagrange's equation as follow we have:

a). The joint equation as:

$$\frac{d}{dt}\left(\frac{\partial T}{\partial \dot{\theta}}\right) - \frac{\partial T}{\partial \theta} + \frac{\partial V_e}{\partial \theta} + \frac{\partial V_g}{\partial \theta} = \tau \qquad (21)$$

or:

$$\mu\left\{\ddot{\theta}\int_0^l \eta^2 d\eta + \sum_{i=1}^{m}\ddot{\delta}_i\int_0^l \eta y_i\, d\eta + 2\dot{\theta}\sum_{i=1}^{m}\sum_{j=1}^{m}\dot{\delta}_i\delta_j\int_0^l y_i y_j\, d\eta\right\}$$

$$- Mg_y r_c C\theta + g_y \mu S\theta\sum_{i=1}^{m}\delta_i\int_0^l y_i\, d\eta = \tau \qquad (22)$$

Where τ is the applied torque at the joint.

b). The deflection equation for the ith mode is:

$$\frac{d}{dt}\left(\frac{\partial T}{\partial \dot{\delta}_f}\right) - \frac{\partial T}{\partial \delta_f} + \frac{\partial V_e}{\partial \delta_f} + \frac{\partial V_g}{\partial \delta_f} = 0 \qquad (23)$$

$$\mu\left\{\sum_{j=1}^{m}\left[\delta_j - \theta^2\delta_j\right]\int_0^l y_i y_j\, d\eta + \ddot{\theta}\int_0^l \eta y_i\, d\eta\right\} \qquad (24)$$

$$+\sum_{j=1}^{m}\delta_j EI_z\int_0^l \frac{\delta^2 Y_j}{\delta\eta^2}\cdot\frac{\partial^2 Y_i}{\partial\eta^2}d\eta - g_y \mu C\theta\int_0^l y_i\, d\eta = 0$$

Equations 22 and 24 may be derived from direct differentiations of Equations 13, 18, and 20, or by Book's formulation presented in [1]. If and only if one mode shape is considered in computations and it is assumed as the first mode of a one-end-fixed cantilever beam [2, 3, 4], we have [8]:

$$y_1(\eta) = -1.362\left[\mathrm{Cos}\left(1.875\frac{\eta}{l}\right) - \mathrm{Cosh}\left(1.875\frac{\eta}{l}\right)\right] \cdot$$

$$+ \mathrm{Sin}\left(1.875\frac{\eta}{l}\right) - \mathrm{Sinh}\left(1.875\frac{\eta}{l}\right) \qquad (25)$$

Computing Equations 22 and 24 for the first mode, the system's equations of motion shall be as:

$$\frac{\mu l^3}{3}\ddot{\theta} + 0.775\,\mu l^2\ddot{\delta} + 3.71\,\mu l\,\dot{\theta}\dot{\delta} - \frac{g_y \mu l^2}{2}C\theta$$

$$+ 1.066\, g_y \mu l\,\delta S\theta = \tau \qquad (26)$$

$$0.775\,\mu l^2\ddot{\theta} + 1.855\,\mu l\ddot{\delta} - 1.855\,\mu l\dot{\theta}^2\delta + 22.928\frac{EI_z}{l^3}\delta$$

$$+ 1.066 g_y \mu l C\theta = 0 \qquad (27)$$

Where θ is the joint angle, δ is the time-varying amplitude of the first mode, μ is the mass per unit length, l is the link length, g_y is the gravitational accelerations, E is the Younge's Modulus of Elasticity, and I_z is the area moment of inertia about the Z-axis.

The Finite Element Approach

In this section we make use of the method introduced by Usoro et. al. [5] for the analysis of flexible robots with rigid joints. They divide each link of the robot into a number of elements, and define a deflection function in terms of the Hermitian polynomials shape function, resulting in inertia and stiffness matrices for each of the elements. Utilizing the above matrices, one can compute the kinetic and potential energies of these elements, and rearrange them to compute the global stiffness and inertia matrices of the robot. Applying boundary conditions and using Lagrange's equations, the differential equations of motion of the system are achieved.

Using the above method (F. E. M.), nonlinear equations of motion of a one link elastic planar robot with one element is presented here (see Figure 2).

The (X_0, Y_0, Z_0) is the inertial coordinate frame and the (X_1, Y_1, Z_1) is the link coordinate frame, where the

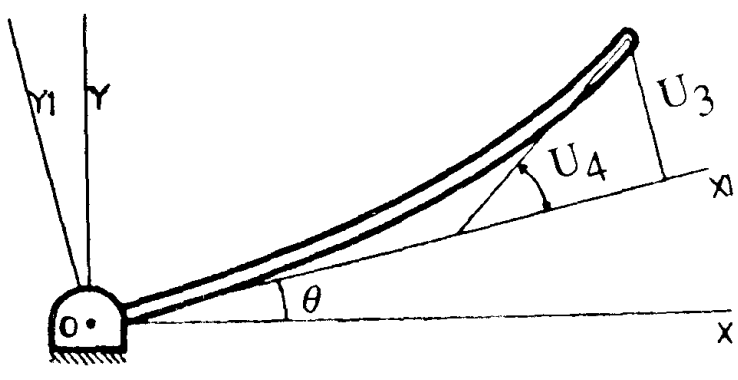

Figure 2. One-link elastic arm with one element.

undeformed link is in the direction of X_1-axis. And U_3 and U_4 represent the flexural displacement and slope of the tip, respectively. Furthermore, U_1 and U_2 are the flexural displacement and slope at the joint in which they are set to zero. As indicated by Usoro [5], the mass matrix of such a robot is given by:

$$\underset{\approx}{M}=\begin{bmatrix} M(1,1)\ M(1,2)\ M(1,3)\ M(1,4)\ M(1,5) \\ M(2,1) \\ M(3,1) \\ M(4,1) \qquad\qquad \underset{\approx}{P} \\ M(5,1) \end{bmatrix} \tag{28}$$

Where:

$$M(1,1)=\frac{ml^3}{3}+\frac{ml}{420}\left[156U_1^2+4l^2U_2^2+156U_3^2+4l^2U_4^2+44lU_1U_2-44lU_3U_4+108U_1U_3+26lU_2U_3-26lU_1U_4-6U_2U_4\right]$$

$$M(1,2)=M(2,1)=\frac{3}{20}ml^2$$

$$M(1,3)=M(3,1)=\frac{1}{30}ml^3$$

$$M(1,4)=M(4,1)=\frac{7}{20}ml^2$$

$$M(1,5)=M(5,1)=-\frac{1}{20}ml^3$$

$$\underset{\approx}{P}=\frac{ml}{420}\begin{bmatrix} 156 & 22l & 54 & -13l \\ 22l & 4l^2 & 13l & -3l^2 \\ 54 & 13l & 156 & -22l \\ -13l & -3l^2 & -22l & 4l^2 \end{bmatrix}$$

The kinetic energy of this robot is formulated as:

$$T=\frac{1}{2}\left[\dot{\theta}\dot{U}_1\dot{U}_2\dot{U}_3\dot{U}_4\right]\underset{\approx}{M}\left[\dot{\theta}\dot{U}_1\dot{U}_2\dot{U}_3\dot{U}_4\right]^T \tag{29}$$

and, the stiffness matrix of this robot is defined as:

$$\underset{\approx}{K}=\frac{EI_z}{l^3}\begin{bmatrix} 12 & 6l & -12 & 6l \\ 6l & 4l^2 & -6l & 2l^2 \\ -12 & -6l & 12 & -6l \\ 6l & 2l^2 & -6l & 4l^2 \end{bmatrix} \tag{30}$$

Finally, the potential energy of the robotic system is represented by:

$$V=mg\frac{l^2}{2}S\theta+mgC\theta\left[\frac{lU_1}{2}+\frac{l^2U_2}{12}+\frac{lU_3}{2}-\frac{l^2U_4}{12}\right]+\frac{1}{2}\left[U_1U_2U_3U_4\right]\underset{\approx}{K}\left[U_1U_2U_3U_4\right]^T \tag{31}$$

Applying the boundary conditions $U_1=U_2=0$, the kinetic and potential energies of the system are reduced to:

$$T=\frac{1}{2}\left[\dot{\theta}\dot{U}_3\dot{U}_4\right]\left\{\frac{ml}{420}\begin{bmatrix} 140l^2+156U_3^2+4U_4^2l^2-44lU_3U_4 & 147l & -21l^2 \\ 147l & 156 & -22l \\ -21l^2 & -22l & 4l^2 \end{bmatrix}\begin{bmatrix} \dot{\theta} \\ \dot{U}_3 \\ \dot{U}_4 \end{bmatrix}\right\} \tag{32}$$

$$V=mg\frac{l^2}{2}S\theta+mgC\theta\left[\frac{lU_3}{2}-\frac{l^2U_4}{12}\right]+\frac{EI_z}{l^3}\left[6U_3^2-6U_3U_4l+2l^2U_4^2\right] \tag{33}$$

Utilizing Equations 32, 33, and the Lagrangian equations, and assuming the inertial matrix is time-invariant, the equation of motion of the robotic system is derived as:

$$\frac{ml}{420}\begin{bmatrix} 140l^2+156U_3^2+4U_4^2l^2-44lU_3U_4 & 147l \\ 147l & 156 \\ -21l^2 & -22l \end{bmatrix}$$

$$\begin{bmatrix} -21l^2 \\ -22l \\ 4l^2 \end{bmatrix} \begin{bmatrix} \ddot{\theta} \\ \ddot{U}_3 \\ \ddot{U}_4 \end{bmatrix} - \begin{bmatrix} -mg\frac{l^2}{2}C\theta + mgS\theta\left(\frac{lU_3}{2} - \frac{l^2U_4}{12}\right) \\ \frac{ml\dot{\theta}^2}{420}(156U_3 - 22lU_4) - mg\frac{l}{2}C\theta \\ \frac{ml\dot{\theta}^2}{420}(4l^2U_4 - 22lU_3) + mg\frac{l^2}{12}C\theta \end{bmatrix}$$

$$\begin{bmatrix} -\frac{EI_z}{l^3}(12U_3 - 6U_4l) \\ -\frac{EI_z}{l^3}(-6lU_3 + 4l^2U_4) \end{bmatrix} = \begin{bmatrix} \tau \\ 0 \\ 0 \end{bmatrix} \qquad (34)$$

PART TWO: NUMERICAL ANALYSIS

Numerical Results

The equations developed from Lagrangian and Finite Element methods are solved for a single link flexible robot with the following specifications:

link length:	$l = 1$ (m)
Mass per unit length:	$\mu = 1$ (kg/m)
Modulus of Elasticity:	$E = 2 \times 10^{11}$ (N/m^2)
Area Moment of Inertia:	$I_z = 1.3 \times 10^{-9}$ (m^4)
Solid Circular rod with diameter:	D = 1.28 (cm)

These equations are numerically solved simultaneously by the Hammings Modified Predictor Corrector Method [9] via Fortran-77 on an IBM-PC-AT computer. The convergence rate for both of these methods is quite different. For various imputs, the Lagrangian method converges two to five times quicker than the F.E.M.. It is noticeable that in F.E.M., the existence of very small elements in the inertia matrix sometimes results in an instability of the solutions. And by eliminating these values, the stability of these equations are improved.

The results obtained from various imputs and initial conditions applied to these equations are analyzed. Only three different examples will be presented here and the reader may refer to Ghassempouri [6] for further details. These cases are as follows:

a) Free motion of robot arm about its equilibrium position (see Figure 3 (a)).

b) Forced motion of robot arm under Step torque input (see Figure 4 (a)).

c) Forced motion of robot arm under Half-Sine torque input (see Figure 4 (b)).

For all three cases, variations of following parameters are sketched vs. time. Where θ_c is the joint angle in the continuum model, θ_f is the joint angle in the F. E. M. model, δ is the mode shape amplitude of the link in the

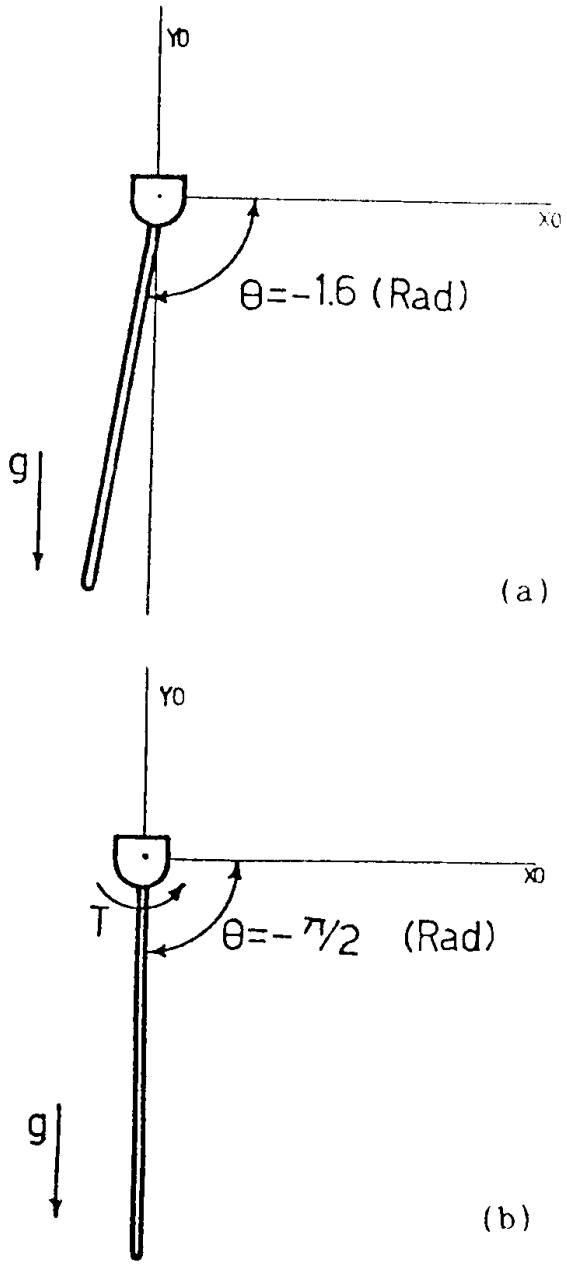

Figure 3. (a) Free motion of the robot.
(b). Forced motion of the robot.

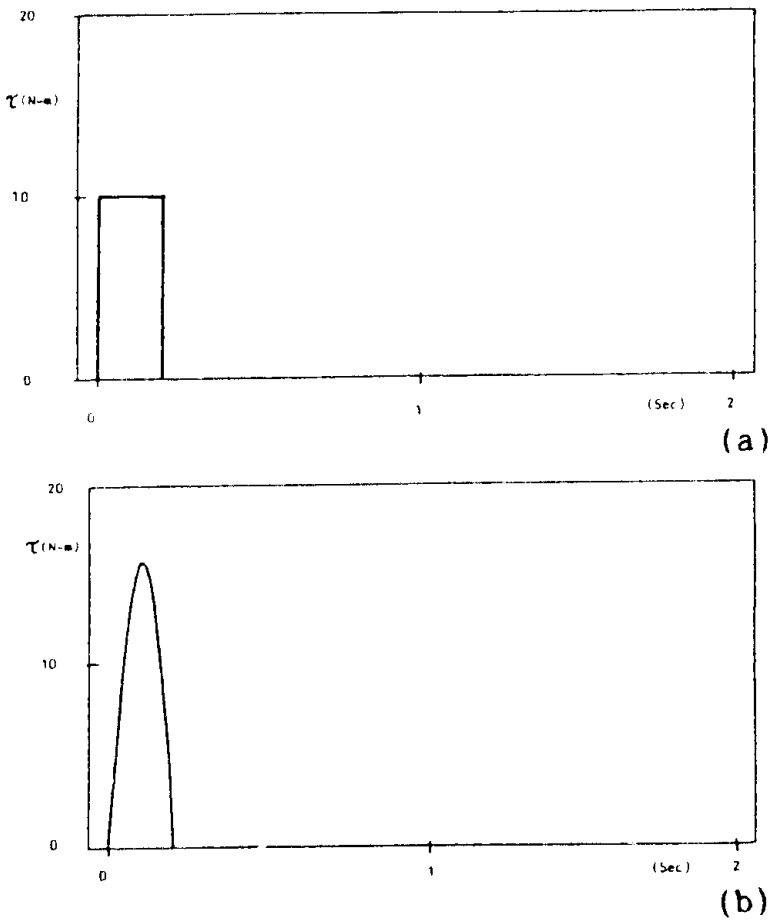

Figure 4. (a). Step torque input.
(b). Half-Sine torque input.

continuum model, and U_3 is the end point deflection of the link in the F. E. M. model. Furthermore, X_c and X_f are the X-components of the link's end point in the continuum and F. E. M. models respectively.

a). Free Motion of the Robot Arm

Considering the arm to be released from the position shown in Figure 3 (a) with a zero input torque at the joint, the resulting motion is represented by Figure 5. Figures 5 (a) and 5 (b) clearly show the variations of θ_c and θ_f which indicate the robot's oscillation about the equilibrium point due to its initial displacement. The period of oscillation of the link angular displacement differs a little in both models. In addition to its own oscillations about the equilibium axis, θ_c vibrates with a low amplitude. This effect is not observed in the F. E. M. model. Figures 5 (c) and 5 (d) show the variations of δ and U_3 respectively, and clearly indicate that the vibrational behavior of both models is similar.

The link deflections observed here are due to two sources; one being the link's structural vibration which is specified by a high frequency, and the other being the change in the robot's configuration in the gravitational field which appears at a low frequency. Figure 5 (e) shows the variation of X_c and X_f which are closely coincident.

b). Robot Arm Motion Under Step Torque Input

Considering the arm with an input torque as shown in Figures 3 (b) and 4 (a), the resulting variations of θ_c and θ_f vs. time are displayed in Figures 6 (a) and 6 (b). Once again in addition to its own oscillations, θ_c vibrates with a high frequency resulting from structural vibrations. The difference in the period of oscillation for both models is more than the case where the robot was in free motion. The reason being an increase in the amplitude of oscillation of the link due to the step input and its effect on the joint angle in the continuum model. Figures 6 (c) and 6 (d) show the variations of δ and U_3. The results obtained for δ in the continuum model match the physical nature of this robot completely. They clearly show the effects of sources (variations in gravitational field and structural vibrations) creating deformations in the link. Unfortunately, the F. E. M. model does not show the same suitable behavior. The obtained results not only do not match the physical nature of the robot, but also in solving the equations numerically, the rate of convergence is lower than the Lagrangian (Continuum) method and the computation time is greater. This especially happens when the applied torque is suddenly removed, resulting in a new shock to the system, and the F. E. M. model faces difficulties.

Figure 6 (e) shows the variations of X_c and X_f. Due to the difference in periods of oscillations of both models, the step input results in high actuation of the system, and furthermore creates a greater difference in behavior of both models.

c). Robot Arm Motion Under Half-Sine Torque Input

Upon application of the torques shown in Figure 4 (b) to the robot, the following results are obtained:

Figures 7 (a) and 7 (b) clearly show the variations in θ_f and θ_c. Due to the soft nature of the applied torque, the disturbance is very little and the difference in behavior of both models is less than the previous case.

Figures 7 (c) and 7 (d) show the variations in δ and U_3 respectively. These figures clearly show a better behavior

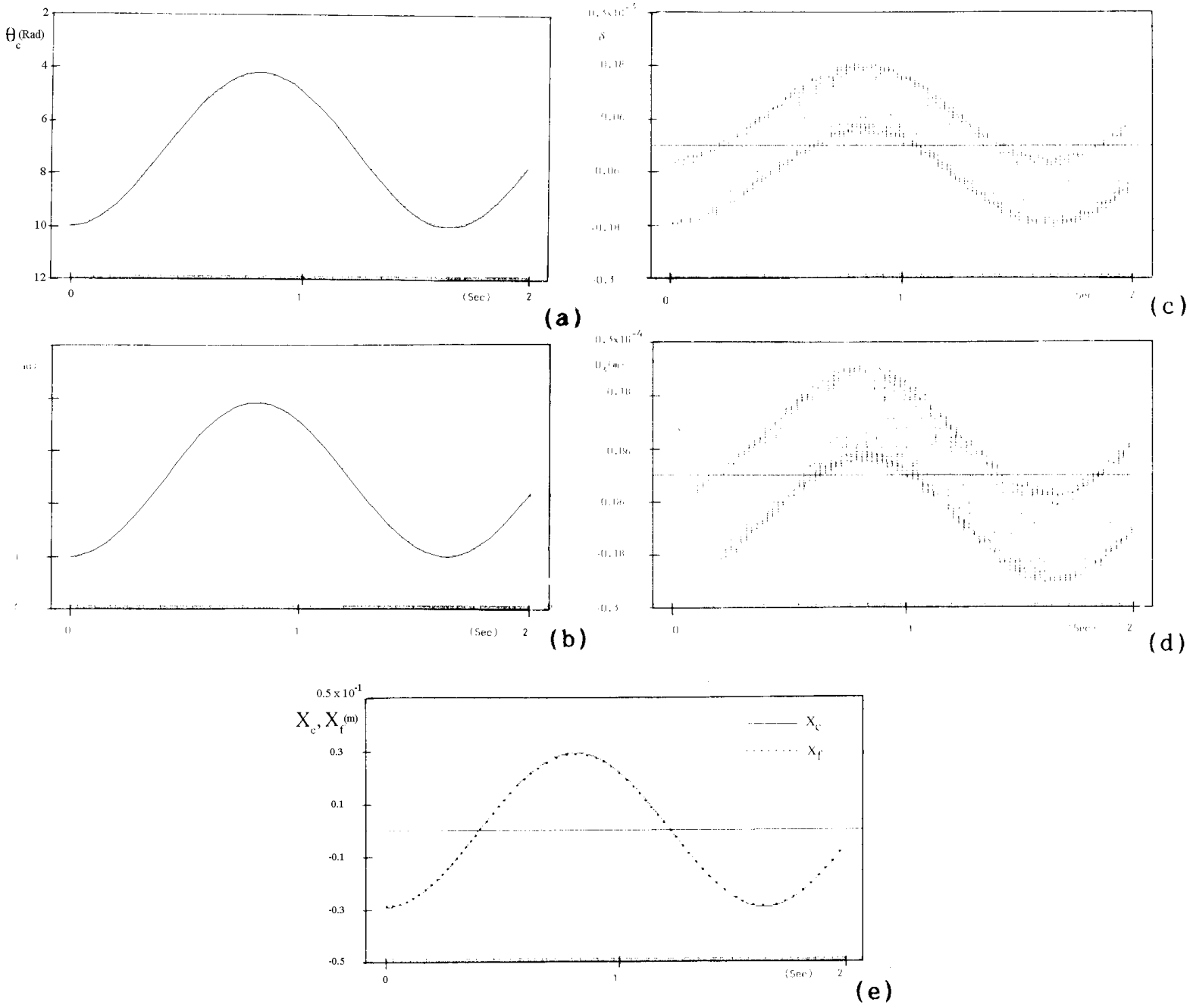

Figure 5. Variations of motion parameters θ_c, θ_f, δ, U_s, X_c, X_f, vs. time under free motion.

of both models. Finally, Figure 7(e) shows the variations of X_c and X_f, which are about the same.

RESULTS: A COMPARATIVE LOOK

Comparing both methods indicates that in the continuum model formulation, there is no need for computing the kinetic and potential energies of the system. The dynamic equations of the system are derived directly using the given formulation. By increasing the number of links, or the number of modes under analysis, the size of corresponding matrices remains fixed and upon general formulation of the robot, one can analyze the robot arm for any number of mode shapes without any need for a new formulation.

In the finite element method, the kinetic and potential energy of the system must be computed and then by applying the Lagrangian equation the equations of motion of the system may be found. In this method as the number of links or mode shapes increase, the size of the matrices involved in computations also increases, and to increase the number of mode shapes, one must reformulate the modeling process and perform the computation all over

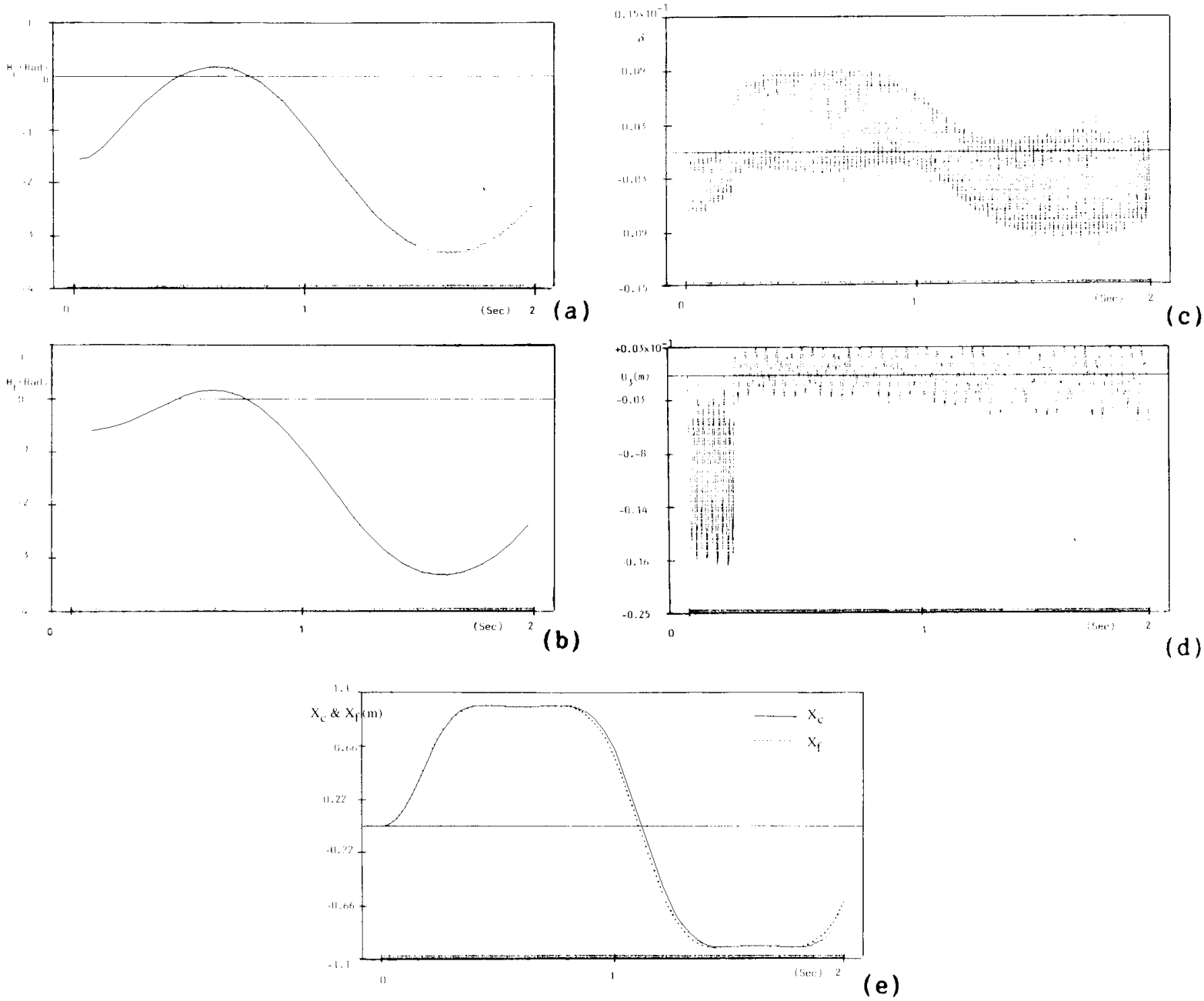

Figure 6. Variations of motion parameters θ_c, θ_f, δ, U_3, X_c, X_f, vs. time under step torque input.

again.

The rate of convergence of equations of motion for the continuum model is two to five times quicker than the F. E. M. model. The sensitivity of the continuum model to the step size is less than the F. E. M. model. In the F. E. M. model, the equations become unstable when the step size is increased. Finally, due to the great amount of computations, the F. E. M. model is slower.

Overall behavior of both models from a mathematical point of view is very similar. Table 1 displays an overall comparison of both models for step and half sine torque inputs.

Another interesting difference between these models is that in Equation 22 developed using continuum model, the term $2\dot{\theta}\dot{\delta}\delta\mu\int_0^l yyd\eta$ is present while there is no similar term in Equation 34 developed by the F. E. M. model. This term is a torque resulted from the Coriollis force at the robot joint (see Figure 8). Existence of this term in the continuum model causes the link structural vibration to affect the joint angle. Hence, in addition to the oscillatory motion about its equilibrium point, the joint angle vibrates with small amplitude which is compatible with its physical nature. But in the F. E. M. model, variation of the mass

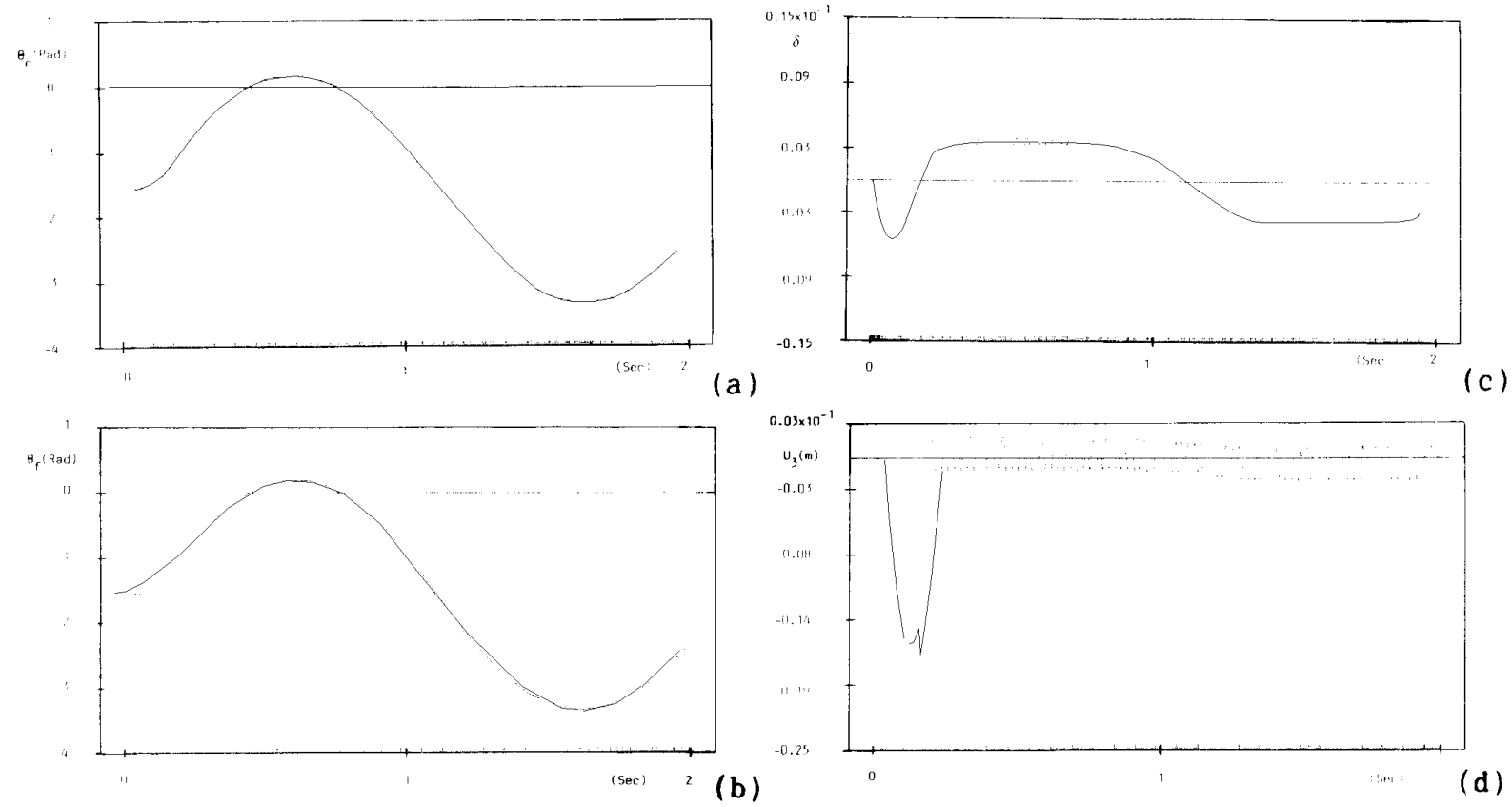

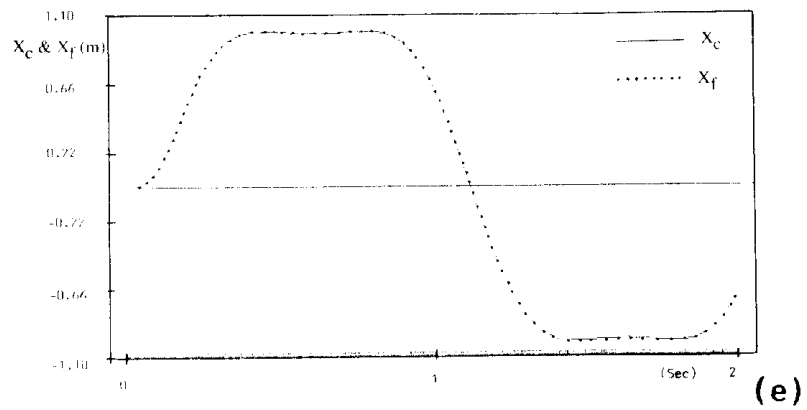

Figure 7. Variations of motion parameters θ_c, θ_f, δ, U_3, X_c, X_f, vs. time under Half-Sine torque input.

Table 1. System Behavior Under Step and Half-Sine Inputs.

Input Type	F.E.M. Model				Continuum Model		
	$X_c - X_f$ max [m]	maximum endpoint deflection [m]	low frequency [Hz]	high frequency [Hz]	maximum endpoint deflection [m]	low frequency [Hz]	high frequency [Hz]
Step	0.003	0.02	0.49	50	0.03	0.48	54
Half-Sine	5×10^{-4}	0.018	0.49	45.5	0.0173	0.49	54

matrix with respect to time was ignored, and as a result the effect of Coriollis force was not considered. Hence, the system behavior using F. E. M. modeling differs from its actual model. In fact, this is the most important difference between the two models.

ANALYSIS OF A TWO LINK FLEXIBLE ROBOT ARM

Comparing the results obtained in previous sections, the continuum model was found to be more suitable for further modeling. Hence, using this formulation the equations of motion of a two-link flexible robot were derived by considering f mode shapes for each link, (see Figure 9). The geometrical and mechanical specifications of both links are exactly the same. The general form of these equations are represented by Equations 35, 36, 37, and 38 in which they are highly non-linear, and their numerical solution is complex and time consuming [6].

For the first joint we have:

$$\frac{d}{dt}\left(\frac{\partial T}{\partial \dot{\theta}_1}\right)-\frac{\partial T}{\partial \theta_1}+\frac{\partial V_g}{\partial \theta_1}+\frac{\partial V_e}{\partial \theta_1}=\tau_1 \qquad (35)$$

For the second joint we have:

$$\frac{d}{dt}\left(\frac{\partial T}{\partial \dot{\theta}_2}\right)-\frac{\partial T}{\partial \theta_2}+\frac{\partial V_g}{\partial \theta_2}+\frac{\partial V_e}{\partial \theta_2}=\tau_2 \qquad (36)$$

For the first link and fth mode we have:

$$\frac{d}{dt}\left(\frac{\partial T}{\partial \dot{\delta}_{1_f}}\right)-\frac{\partial T}{\partial \delta_{1_f}}+\frac{\partial V_g}{\partial \delta_{1_f}}+\frac{\partial V_e}{\partial \delta_{1_f}}=0 \qquad (37)$$

For the second link and fth mode we have:

$$\frac{d}{dt}\left(\frac{\partial T}{\partial \dot{\delta}_{2_f}}\right)-\frac{\partial T}{\partial \delta_{2_f}}+\frac{\partial V_g}{\partial \delta_{2_f}}+\frac{\partial V_e}{\partial \delta_{2_f}}=0 \qquad (38)$$

These equations are solved numerically for various cases, but only the results obtained from free motion about the equilibrium position are presented here (see Figure 10).

The variation in joint angles θ_{1c} and θ_{2c}, the mode shapes' amplitudes of the first and second links δ_1 and δ_2, and the X-component value of the tip of the robot are shown in Figure 11.

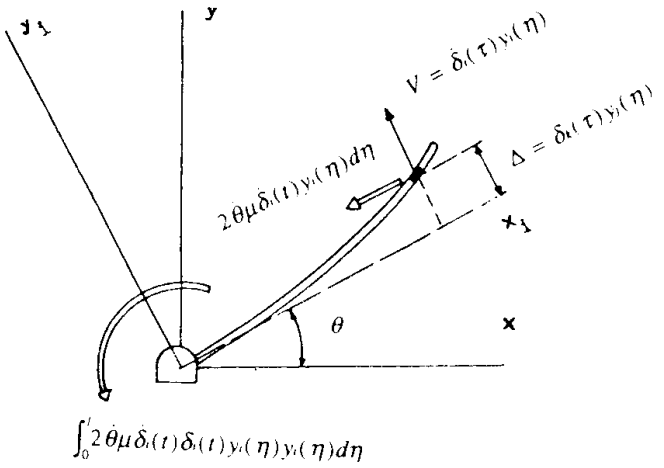

Figure 8. Effect of coriollis force in continum model.

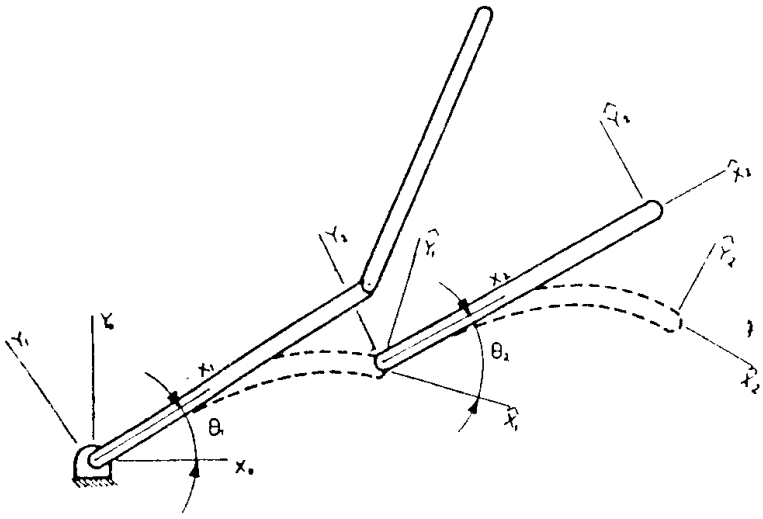

Figure 9. The two-link flexible arm.

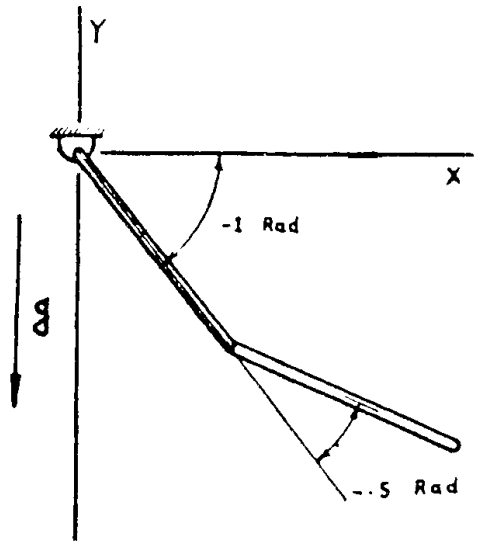

Figure 10. Free of the two-link arm.

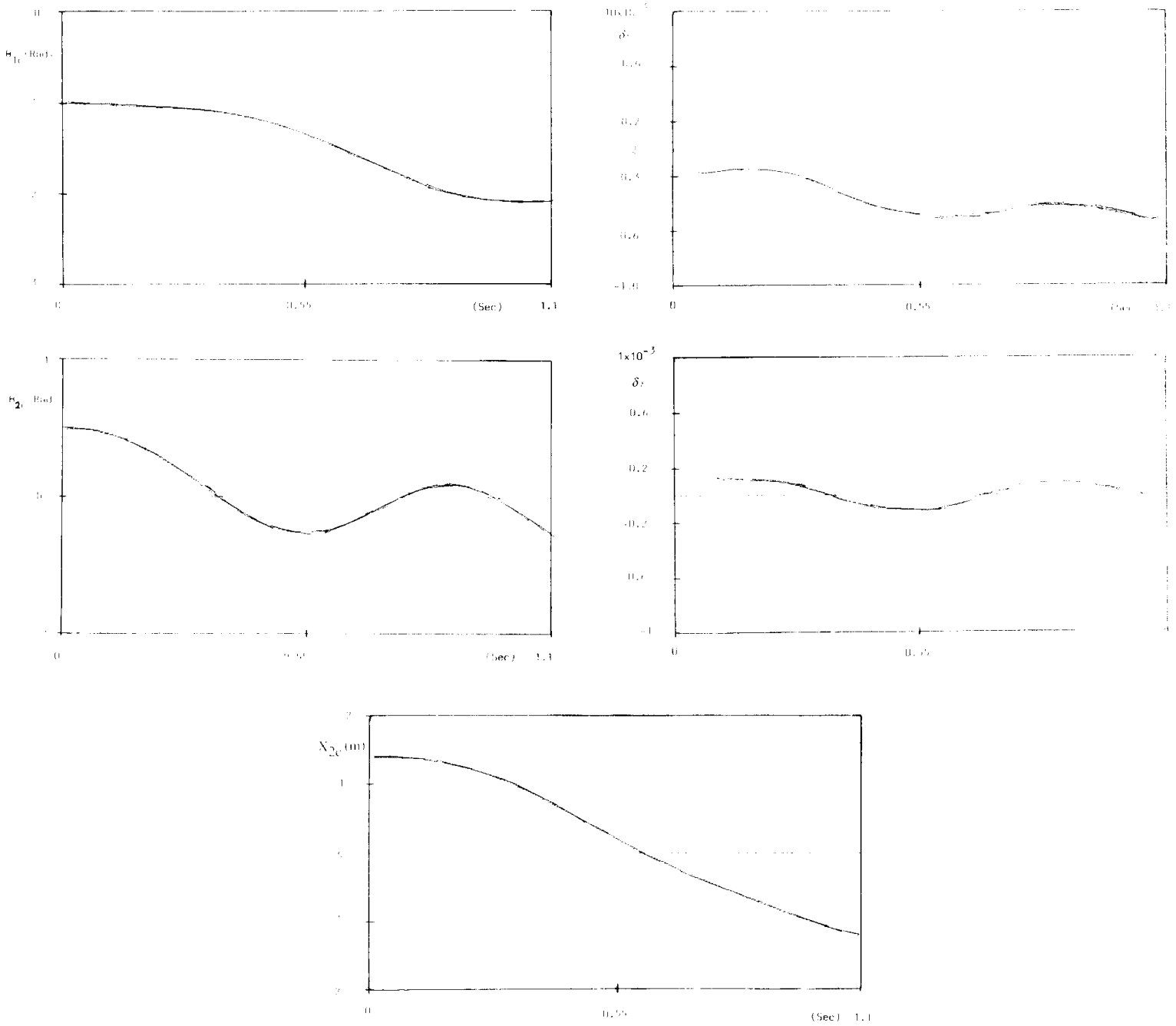

Figure 11. Variations of motion parameters θ_{ic}, θ_{2c}, δ_1, δ_2, X_{2c} vs. time under free motion of the arm.

CONCLUSIONS

Equations of motion of a one-link flexible arm were derived using the Continuum and Finite Element Modelings. These equations in the presence of various inputs were solved numerically and the results are presented. The obtained numerical results indicate that the continuum approach is a more suitable model than the F. E. M. modeling. Using this conclusion, equations of motion of a two-link flexible arm were derived by the Continuum model. Obtained equations were solved numerically and the results are presented.

REFERENCES

1. W.J. Book, *Int. J. of Robotics Research*, vol. 3, no. 3, pp. 87-101 (1989).
2. W.J. Book, O. Maizza-Neto, and D. E. Whitney, *Trans ASME J. of Dynamic Systems, Measurment & Control*, 97, pp. 424-431 (1975).

3. W. J. Book, "Modeling, Design and Control of Flexible Manipulator Arms", Ph. D. Thesis, M. I. T., Department of Mechanical Engineering, USA (1974).
4. G. G. Hastings and W. J. Book, *IEEE Control Systems Magazine*, pp. 61-64 (1987).
5. P. B. Usoro, R. Nadira and S. S. Mahil, *Trans. ASME J. Dynamic Systems, Measurment & Control*, vol. 108, pp. 198-205 (1987).
6. M. Ghassempouri, "Modeling, Dynamics, and Control of Flexible Robots", M. Sc. Thesis, Sharif University of Technology, Department of Mechanical Engineering, Iran (1991).
7. A. Meghdari, "A Variational Approach for Modeling Flexibility Effects in Manipulator Arms", *Robotica Int. J.* vol. 9, pp. 213-217 (1991).
8. F.S.Tse, I.E.Morse and R.T.Hinkle, "Mechanical Vibrations Theory and Applications", Allyn and Bacon Inc. (1987).
9. W. Ralston, "Mathematical Methods for Digital Computers", Wiley, New York & London, pp. 95-109 (1960).
10. S. Timoshenko and J. Goodier, "Theory of Elasticity", 3rd Ed., McGraw-Hill Book Co., New York, (1970).